Investigating the influence of the grain size and distribution on the macroscopic dielectric properties of Antarctic firn

Published:
DOI: http://doi.org/10.1016/j.coldregions.2021.103254

R. Olmi, M. Bittelli, G. Picard, L. Arnaud, A. Mialon, S. Priori,
Investigating the influence of the grain size and distribution on the macroscopic dielectric properties of Antarctic firn,
Cold Regions Science and Technology, Volume 185, 2021, 103254, ISSN 0165-232X,
The final published version is available online at:
https://doi.org/10.1016/j.coldregions.2021.103254.

Cold Regions Science and Technology

Investigating the influence of the grain size and distribution on the macroscopic dielectric properties of Antarctic Firn

--Manuscript Draft--

Manuscript Number:	
Article Type:	Research Paper
Keywords:	Antarctica, dielectric measurements, ice cores, dielectric model, full wave EM simulations, firn
Corresponding Author:	MARCO BITTELLI University of Bologna Bologna, WA ITALY
First Author:	Roberto Olmi, PhD
Order of Authors:	Roberto Olmi, PhD
	MARCO BITTELLI
	Ghislain Picard, PhD
	Laurent Arnaud, PhD
	Arnaud Mialon, PhD
	Saverio Priori, PhD
Abstract:	This study is based on the analysis of detailed measurements of firn dielectric properties performed in Antarctica through coring down to 106 meters. Dielectric measurements in the frequency band (0.4 - 2.5 GHz) have been carried out using an open-resonator probe. Density was also measured for the same samples. The experimental results confirmed the well-known dependence of the real part of permittivity ε ' on depth and density, showing an increase of ε ' with density. The imaginary part also increases with depth with a rather complex dependence on frequency, probably due to the presence of salts or impurities. The analysis of the experimental data was performed by implementing 3D and 2D full wave numerical models, to simulate a mixture of firn crystals at prescribed densities, corresponding to the measured densities on the ice cores. The numerical analysis of the ensemble of inclusions showed that the usual symmetric formulae used for modeling ice dielectric properties agree with the average results of the simulation but they are not able to explain the spreading of the measured data at given density. A dielectric model was developed allowing for quantification of the dependence of dielectric properties on density, by combining two models: one consisting in firn crystals into an air host, the other assuming the presence of air inclusions into an homogeneous firn host. The weighted equation is based on the volume fraction. A simple geometric shape (ellipsoidal) is assumed for both ice crystals and air inclusions. This kind of shape is reasonable for the purpose of the dielectric study. The result is a mixture, smoothly changing from firn particles in air (low density) to air bubbles in an ice matrix (high density). A statistical analysis has been accomplished to investigate the dependence of the dielectric properties on the geometrical arrangement of the inclusions. For that purpose, a large number of simulations with different arrangements (micro-states) giving rise to the same average density (macro-state) has been carried out. The permittivity change due to micro-state variability appears to be at least two-three times the model variation due to density alone, and comparable to the measured variability at a given depth, suggesting that firn structure has a significant effect on the dielectric properties.
Suggested Reviewers:	Udo Kaatze, PhD Professor, Georg-August-Universität Göttingen udo.kaatze@phys.uni-goettingen.de World leading expert in dielectric spectroscopy and EM methods
	Frank Daschner, PhD Chair of Microwave Engineering, Christian-Albrechts-Universitat zu Kiel

	fd@tf.uni-kiel.de Expert on microwave spectroscopy and engineering. Published many papers on cavity resonators (used in this study) on a variety of media.
	Yuri F Feldman, PhD Professor, Hebrew University of Jerusalem yurif@vms.huji.ac.il World expert in the field of EM methods and dielectric spectroscopy. Authors of books and many papers. Performed research and published on the dielectric properties of snow and ice.
	Tuami Lasri, PhD Professor, NRC National Institute for Nanotechnology tuami.lasri@iemn.univ-lille1.fr Expert in dielectric spectroscopy and micro electronics. He published many papers on dielectric spectroscopy and modelling.
	Shin SUGIYAMA, PhD Professor, Hokkaido University sugishin@lowtem.hokudai.ac.jp Expert on Antarctic firn. He performed research on dielectric measurement on Antarctic Ice. Performed extended meaasuring campaigns.

Investigating the influence of the grain size and distribution on the macroscopic dielectric properties of Antarctic Firn

R. Olmi[1], M. Bittelli[2], G. Picard[3], L. Arnaud[3], A. Mialon[4], and S. Priori[1]

[1]Istituto di Fisica Applicata (IFAC), Consiglio Nazionale delle Ricerche (CNR), Sesto Fiorentino, Italia

[2]Dipartimento di Scienze e Tecnologie Agro-Alimentari (DISTAL), Università di Bologna, Italia

[3]UGA, CNRS, Institut des Géosciences et de l'Environnement (IGE), Grenoble, France

[4]CESBIO, Université de Toulouse, CNES/CNRS/INRAE/IRD/UPS, Toulouse, France

April 2020

1 Abstract

This study is based on the analysis of detailed measurements of firn dielectric properties performed in Antarctica through coring down to 106 meters. Dielectric measurements in the frequency band $(0.4 - 2.5$ GHz$)$ have been carried out using an open−resonator probe. Density was also measured for the same samples. The experimental results confirmed the well−known dependence of the real part of permittivity ϵ' on depth and density, showing an increase of ϵ' with density. The imaginary part also increases with depth with a rather complex dependence on frequency, probably due to the presence of salts or impurities.

The analysis of the experimental data was performed by implementing 3D and 2D full wave numerical models, to simulate a mixture of firn crystals at prescribed densities, corresponding to the measured densities on the ice cores. The numerical analysis of the ensemble of inclusions showed that the usual symmetric formulae used for modeling ice dielectric properties agree with the average results of the simulation but they are not able to explain the spreading of the measured data at given density.

A dielectric model was developed allowing for quantification of the dependence of dielectric properties on density, by combining two models: one consisting in firn crystals into an air host, the other assuming the presence of air inclusions into an homogeneous firn host. The weighted equation is based on the volume fraction. A simple geometric shape (ellipsoidal) is assumed for both ice crystals and air inclusions. This kind of shape is reasonable for the purpose of the dielectric study. The result is a mixture, smoothly changing from firn particles in air (low density) to air bubbles in an ice matrix (high density).

A statistical analysis has been accomplished to investigate the dependence of the dielectric properties on the geometrical arrangement of the inclusions. For that purpose, a large number of simulations with different arrangements (micro−states) giving rise to the same average density (macro−state) has been carried out. The permittivity change due to micro−state variability appears to be at least two−three times the model variation due to density alone, and comparable to the measured variability at a given depth, suggesting that firn structure has a significant effect on the dielectric properties.

Keywords: Antarctica, dielectric measurements, ice cores, dielectric model, full wave EM simulations, close-off, firn

2 Introduction

Remote sensing techniques employed to measure Antarctica ice thickness, such as as radars or radiometers, require an accurate estimation of ice dielectric properties. The real and imaginary part of ice permittivity is one of the most important variables determining the penetration depth or scattering of EM waves.

A variety of studies have been presented in the last decades to propose models of electric permittivity of snow and firn. An early work by Polder and van Santen (1946) computed the effective permittivity of a material consisting of a host medium in which solid particles or empty holes, assumed of ellipsoidal shape, are packed together. Tiuri et al. (1984) measured the complex permittivity of firn at microwave frequencies, concluding that it is practically independent of the microstructure for density up to 500 kg m^{-3}. Matzer (1996) measured the permittivity of dry snow in 90 samples at different sites in the Swiss and Austrian Alps and showed the strong dependence of the real part of snow permittivity on density. The author also presented a formulation based on the effective medium formula (Polder and van Santen, 1946), and he concluded that the formulation for oblate spheroidal particles was the most appropriate and that the structure of the firn crystals have an effect on permittivity.

The transition between snow, firn and ice is based on density. Firn becomes ice when the interconnecting air− or water−filled passageways between the grains are sealed off, a process called pore close-off. This value depends on density and it usually occurs around a density of 830 kg m^{-3} (Cuffey and Paterson, 2010). In this study we will refer to firn, since the measured densities are usually below this threshold.

A general overview of the different electromagnetic mixing models was presented by Sihvola (1999), discussing a variety of approaches including classic mixing approaches, homogeneous and in−homogeneous inclusions, isotropic and anisotropic media and others. Among the various models, the continuous or bi−continuous random structure models showed promising results in the interpretation and modeling of dielectric spectroscopy or remote sensing data. Karkkainen et al. (2000) presented a numerical analysis of electromagnetic fields in random dielectric materials. The calculated permittivity distribution were compared with theoretical mixture models. They concluded that all the possible permittivity values lie between the Wiener limits, and the values were almost always between the Hashin−Shtrikman limits.

When studying the dielectric properties of firn the most relevant variables are the density, at a macroscopic level, and orientation, size and shape of ice crystals on a microscopic scale. The crystal size can be represented by the average crystal area (Jun and Jacka, 1999), defined as the surface of an ellipse whose long and short semi-axes correspond to the radii of the largest inscribed circle and the smallest circumscribed circle, respectively, for a given crystal. The average crystal area of Antarctic firn is a function of depth. Crystal orientation, expressed for example by the crystallographic c-axis, has been shown to be practically random in polar ice cores (Jun and Jacka, 1999). If the crystal is roughly represented by an ellipsoid, which is acceptable for the purpose of the dielectric model, another parameter possibly influencing permittivity is the aspect ratio, which is descriptive of the crystal shape.

From the dielectric point of view, firn is modeled as a binary mixture, made of "pure" firn/ice and air. Different approaches (Sihvola, 1999) bring to symmetric formulae, where inclusions and host can be interchanged with no consequence on the effective permittivity, or to non−symmetric formulae based on the Maxwell Garnett theory, where the host material is that having the dominant volume fraction.

An analytic formula is only able to represent the average measured dielectric constant as a function of density or volume fraction. The choice of a non−symmetric model involving firn inclusions in air appears reasonable for low−density material, while it does not appear meaningful for high−density material where a suspension of air bubbles into an ice host is physically more based. No analytic formula is able to handle inclusions having different shapes, size and orientation. Therefore a numerical method of analysis is needed.

Direct measurements of the dielectric properties of Antarctic ice, such as “dielectric profiling” (DEP) measurements on sampled firn cores, are scarcely common in the literature. The first comprehensive measurement was performed by Moore (1988), with a profiled firn core of 130 m depth in Antarctica, to measure the reflection coefficient and electrical conductivity to derive the dielectric properties. However, the measurement was limited to the range of 20 Hz to 300 kHz. Wolff et al. (1997) and Wolff (2000) focused on conductivity measurements, but the early attempts to measure firn’s permittivity by DEP (Moore, 1988) were not pursued with more extensive campaigns and at higher frequencies of interest for space-borne radar and radiometers. Suguyama et al. (2010) measured the permittivity of the upper 1 meter snow layer at 35 locations, along a transect of approximately 50 km, using a transmission−line resonator. The measurements provided information in the horizontal direction, but to a shallow depth of 1 meter. Grimm et al. (2015) analyzed dielectric spectra (0.1 Hz − 1 MHz) of 49 firn samples in Antarctica. However, they did not explore higher frequencies and did not collect detailed and extensive measurement on a single core down to over 100 meters depth. Overall, there is need to obtain detailed DEP in depth (at least at up to the close−off) in the frequency bands where space-borne radar and radiometers operate.

This study reports the results of direct measurement of dielectric properties, density and specific surface area, performed at Dome−C in Antarctica (Concordia Experimental Station) down to 106 meters, through the collection of firn cores. The dielectric measurements were performed by an open−resonator probe (Olmi et al., 2019), providing high accuracy measurements of both the real and the imaginary parts, in four narrow frequency bands around 400, 880, 1100 and 2500 MHz, as a function of depth z and density ρ. Measurements of the complex permittivity of firn were performed in situ and later repeated on the same samples transported in a cold laboratory. For the aim of interpreting the variability of experimental permittivity at given density, two− and three− dimensional numerical models has been implemented, based on the Finite Element (FE) method. Computed dielectric permittivities are compared to experimental data and to existing mixture models to obtain a formulation for firn permittivity allowing to take in account the variability due to the microscopic arrangement of firn crystals.

3 Materials and Methods

The dielectric measurements described here have been conducted at the Concordia Station in Antarctica (73^{o}30'S 123^{o}00'E), on a core of firn drilled down to 106 meters depth. Measurements were performed on core slices of 10 cm thickness, whose density was also measured and recorded. A total of 930 samples have been measured *in situ*, i.e. one every 10 cm, with two different open−coaxial resonant probes, the first operating at about 900 MHz in air (2700 MHz in second harmonic), the second at 400 MHz in air (1200 in second harmonic). Measurements concerned depths from about 3 to 106 m, because the first 3 meters of core were damaged. Sample temperature was -20 $^{\mathrm{O}}$C. The samples were later moved into a cold laboratory in Firenze (Italy), where measurements were repeated at -19 $^{\mathrm{O}}$C, on 92 samples spaced about 1 m between them. In both cases only one point per sample was measured, with the exception of a limited number of them for testing purposes.

The electromagnetic technique used for dielectric measurement, based on a open−resonator probe, is thoroughly described in Olmi et al. (2019). The frequency band of interest for the study is 400−2500 MHz, because of the remote sensing applications relevant for the study itself.

The density of the samples used for dielectric measurements was directly deduced from mass and volume measurements. The diameter and height of each sample, assumed to be cylindrical in shape, were measured with a caliper, and mass was measured with a precision balance. Largest uncertainty came from the volume measurement, and accuracy of such density measurements on cohesive firn core samples is estimated to be better than 10 %.

In this work we will not be concerned with the variation of dielectric properties with frequency, the attention being focused on the dependence of permittivity on firn structure at a fixed frequency. Therefore, we will refer all future considerations to a nominal frequency of 1 GHz, although the data are shown for the measured frequencies.

4 Theory

4.1 Numerical Simulation

The dielectric model consists in a host medium containing a random distribution of inclusions (spheres, ellipsoids), of different size and orientation, possibly overlapping. The host medium can be air and the inclusions ice crystals, or the opposite. Borrowing the notion from statistical physics, we define "micro−state" a specific geometrical arrangement of inclusions. The average physical properties (the "macro−state") are obtained in principle by averaging on all possible micro−states. Therefore, generating geometrical arrangements corresponding to the same material density, we can compute the macro−state permittivity by averaging on the micro−states. At the same time, by looking at the statistical distribution of the micro−state permittivity we obtain information on the influence of the geometrical arrangement on the complex permittivity variation.

Both three−dimensional (3D) and two−dimensional (2D) models have been implemented. The composite material fills a section of a parallel−plate wave−guide supporting a transverse electromagnetic (TEM) propagation mode. In the 3D case, the parallel−plate guide is realized by imposing a "perfect−magnetic wall" condition on two surfaces normal to the magnetic field vector, as shown in Figure 1. The EM wave, propagating along the y direction, has the electric field polarized in the z−direction and the magnetic field in the x−direction. The input port is the y=0 plane, while a perfect electric reflector is placed at a distance d from it.

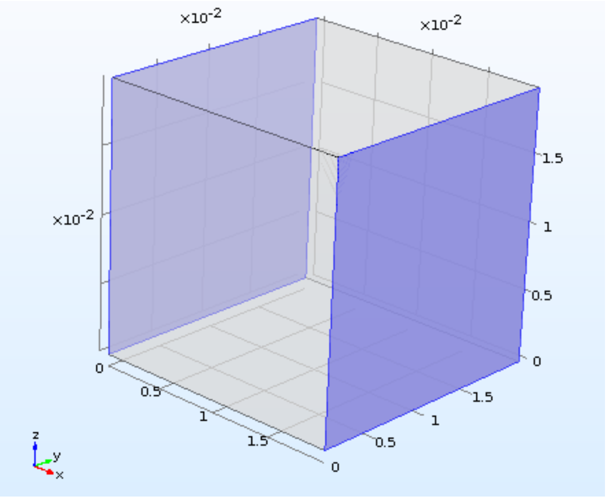

Figure 1: Geometry of the TEM waveguide. Electric field is z−directed, magnetic field is x−directed, wave propagation is along y. The "grayed" surfaces are the perfect magnetic walls.

Computing permittivity by means of the 3D model is very time−consuming, in particular for densities that require a large partial volume fraction of the "inclusion" phase. The statistical analysis to be performed on the ensembles of micro−states, requires the electromagnetic computation to be repeated hundreds of times for a given density value. It was observed that, for a given density, the distribution of the real and imaginary parts are practically identical for a 3D model of prolate spheroids and for a 2D model of ellipses, having semi−axes and orientation in the same range of values. As an example, figure 2 respectively refer to 3D and 2D distributions giving rise to a firn density of 800 kg m^{-3}.

The difference among 3D and 2D simulation is not only in the additional dimension of the former, which dramatically increases the number of degrees

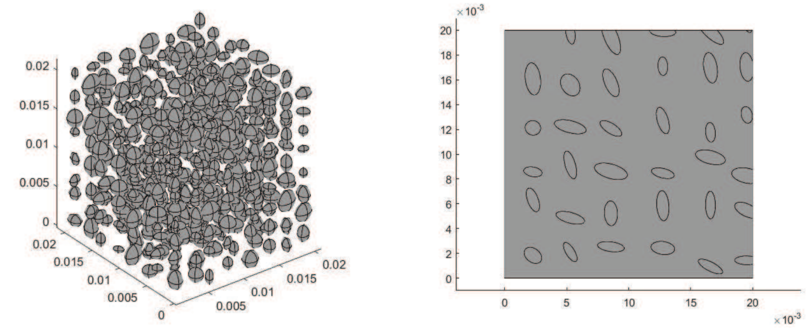

Figure 2: 3D distribution of spheroids and 2D distribution of ellipses (air inclusions in firn) corresponding to an firn density of 800 kg m^{-3}.

of freedom of the FEM problem (or, in other terms, the order of the system of equations to be solved). Both in the 3D and 2D case, the inclusions are modeled as geometric parts and, as such, they require to be meshed (with tetrahedra in the 3D case or triangles in 2D). As a consequence, a geometry having a large number of inclusions, possibly overlapping, requires a huge number of mesh elements. Our approach, in the 2D case, is to generate the proper geometry (i.e. the distribution of inclusion giving the required average density of firn) and to include the information about the inclusion topology in a space−dependent permittivity $\epsilon(x, y)$, which is a continuous analytical function. Although that function has sharp edges at the interface between two materials (host/inclusion), the geometry and the mesh topology of the problem remain unchanged.

Table 1 shows the differences between 2D and 3D for 400 micro−states, for a material having a density $\rho = 800 \pm 0.36\%$ kg m^{-3}.

The almost perfect equivalence among 3D and 2D models suggests re-

Table 1: Comparison between the 3D and 2D mode

3D		2D	
ϵ’	ϵ”	ϵ’	ϵ”
$2.8 \pm 2.5\%$	$1.25 \times 10^{-3} \pm 4.7\%$	$2.8 \pm 2.3\%$	$1.32 \times 10^{-3} \pm 4.5\%$

sorting to a 2D model for the statistical purpose. The electromagnetic model used to compute the complex permittivity of firn is reduced to a section of parallel−plate waveguide, excited at one end (input port) by a TEM mode and short−circuited at the other end (Figure 3).

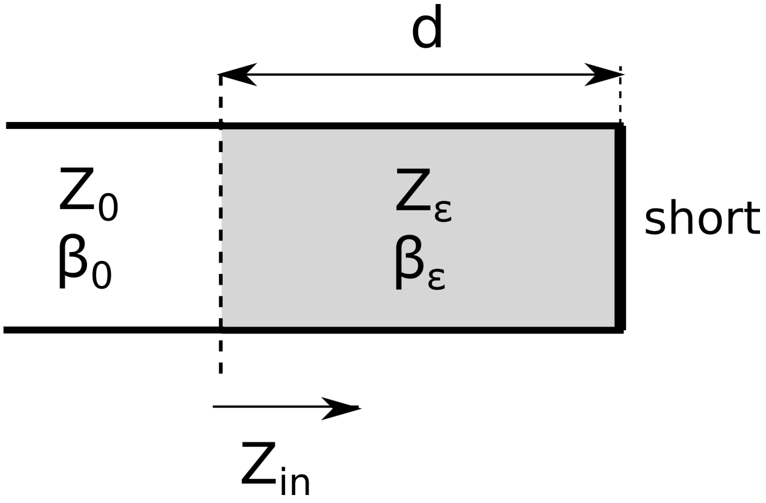

Figure 3: Transmission line equivalent circuit of the plane−wave propagation problem

The complex reflection coefficient computed at the input port contains the information about the permittivity of the material filling the waveguide. The choice of a full−wave solution, analogous to what proposed in Karkkainen et al. (2000), has been preferred to the quasi−static approach proposed by Tuncer et al. (2001) and frequently used in the modeling of random media, e.g. in Zhao et al. (2004). The reason is that while the scale of the inclusions is such to fulfill the requirements for a quasi−static approximation at about 1 GHz, the necessity of having a sufficient volume (surface in 2D) to include a suitable number of firn particles of different size brings to a macroscopic dielectric sample whose size is not sufficiently smaller than the wavelength in firn. If the mean surface of the inclusions is in the order of 1 mm^2, simulating firn with porosity 0.5, a sample surface of 1000 mm^2 contains 500 inclusions. Assuming a rectangular sample surface, the characteristic length (CL) is in the order of the square root of 1000, which is about 1/10 of the wavelength in air, and 1/6 of the wavelength (λ) in firn. These values are too large for a quasi−static approximation, requiring at least CL $< \lambda/20$.

The reflection coefficient at the input of the firn−filled space is computed in terms of the impedance $Z_{in} = jZ_\epsilon \tan(\beta \mathrm{d})$ at the same interface:

$$\Gamma_{in} = \frac{Z_{in} - Z_0}{Z_{in} + Z_0} = \frac{j\tan(\beta \mathrm{d}) - \sqrt{\epsilon}}{j\tan(\beta \mathrm{d}) + \sqrt{\epsilon}} \tag{1}$$

where:

$$\beta = k_0\sqrt{\epsilon} \tag{2}$$

$$Z_\epsilon = Z_0/\sqrt{\epsilon} \tag{3}$$

are the complex wave number and characteristic impedance in firn, respectively, while k_0 and Z_0 are the same quantities in air. The reason for including a "virtual" section in air (actually, it is zero length) is that the FEM code normalizes the computed scattering parameters to the free space impedance. The algorithm for computing the complex permittivity ϵ uses a FEM engine, based on COMSOL Multiphysics®, integrated in MATLAB® code by LiveLink®.

The procedure for computing ϵ is the following. Given the desired density value ρ_D, distributions of ellipses with random orientation (between 0 and $\pi/2$) are generated to fulfil a requirement about the "computed" density $\rho_C = \rho_D \pm \Delta$. An algorithm was written in MATLAB® to generate a certain number of particles of variable size and shape at spatial intervals (fixed on physical basis, as described later), to achieve a target density corresponding to the measured density as function of depth. During the iterations the algorithm adjusts the lengths of the semi−axes, the aspect ratio (AR) and the angle of the generated ellipses.

The complex permittivity ϵ computed inverting (1) for density values ρ_C belonging to the interval $(\rho_D - \Delta, \rho_D + \Delta)$ automatically takes into account the dependence on density. The operation of inverting (1) maps the Γ interval onto an ϵ interval, depending on the density variation:

$$(\Gamma(\rho_D - \Delta),\ \Gamma(\rho_D + \Delta)) \rightarrow (\epsilon(\rho_D - \Delta),\ \epsilon(\rho_d + \Delta))$$

In relatively shallow firn the average crystal area (ACA) of Antarctic firn/ice increases about linearly with depth. From Lipenkov et al. (1989) and Jun and Jacka (1999) the ACA changes from about 0.4−0.9 mm^2 at a depth of

10 m to 1.4−1.6 mm^2 at 100 m. Arnaud et al. (1998) presented experimental data and a physical model (Arnaud et al., 2000) on the transformation of dry snow to firn and the of snow/firn and ice in the upper part of the polar sheets. Few data are available concerning the dependence of crystal orientation on depth for shallow firn, but it is reasonable (see, for example Jun and Jacka (1999)) to assume a random orientation for the $c-axis$. Moreover, the orientation of elliptical inclusions does not have a marked effect on the average permittivity in a medium with randomly oriented inclusions (Sihvola, 1999), as an expected effect of the random dipole polarization moment. That characteristic has been confirmed by the numerical simulations described later in this paper.

In Azuma et al. (1999) the aspect ratio at the lowest reported depth (about 100 m) is about 1.7. We can reasonably assume a linear dependence of the average aspect ratio between 1 and about 2 from the surface to 100 m depth, as an effect of firn compression.

For each density, a number (*e.g.* 100) of simulations are conducted to investigate the dependence of the dielectric properties on the micro−state configurations. From experiments, the dependence of density with depth is known. For each couple (depth, density) set in the numerical model, the average aspect ratio and the average particle diameter is fixed, and two sets of simulations are performed: one involving firn inclusions in air host medium, the other involving air inclusions in an ice host medium.

4.2 Dielectric mixing formulae

The effective permittivity of a random mixture (Sihvola, 2000) cannot be summarized by a closed−form analytic expression, although some work on the analytical treatment of a dielectric containing random metallic inclusions has been done in the recent past (Koledintseva et al., 2006).

The results from numerical simulations of random inclusions in a host material do not agree with homogenisation formulas like that of Bruggeman (Sihvola, 1999) or, which is the same, the frequently used formula derived from the theory developed by Polder and van Santen (1946). The reason is that such formulae are symmetric in the permittivity of the inclusion material (ϵ_i) and of the host environment (ϵ_e):

$$(1-v)\frac{\epsilon_e-\epsilon_m}{\epsilon_e+2\epsilon_m}+v\frac{\epsilon_i-\epsilon_m}{\epsilon_i+2\epsilon_m}=0 \tag{4}$$

where ϵ_m is the (effective medium) mixture permittivity and v is the volume fraction of the inclusion material. Numerically simulated dielectrics do not exhibit such a symmetry: the effective permittivity of an arrangement of ice inclusions in air, computed as a function of the density, is different from the permittivity of an arrangement of air inclusions in ice. As a consequence, if the inclusions were supposed to all have the same shape, the generalized Maxwell Garnett (MG) approach for ellipsoidal inclusions would be the correct choice (Sihvola, 1999). Actually, the MG formula is inherently non symmetrical so, given the density ρ of the material, and computing the air volume fraction v (ρ_I

is the density of pure ice):

$$v = \frac{\rho_I - \rho}{\rho_I - 1} \tag{5}$$

leading to two different dielectrics: (1) an ice bulk medium containing a volume fraction v of air, or (2) an arrangement of firn inclusions having a total volume fraction $1 - v$, in air. Dielectrics (1) and (2) are described by two different MG formulas.

Just to show the connection between the MG approach and the Bruggeman formula, suppose the inclusions are oblate spheroids with semi$-$axis a and b in the ratio $\theta = b/a = 2$. The dielectric constant ϵ_i, assumed real, of the inclusions can be that of ice (3.15) or air (1). Correspondingly, the dielectric constant of the external medium ϵ_e will be 1 and 3.15, respectively.

Given the spheroid eccentricity $e = \sqrt{\theta^2 - 1}$, the MG formula for random inclusions involves the depolarization factors along axes parallel to the main directions (denoted by the numerals 1 to 3), given by (Sihvola, 1999):

$$\begin{aligned} A_1 &= \frac{1+e^2}{e^3}(e - \tan^{-1}(e)) && (6) \\ A_2 &= \frac{1-A_1}{2} && (7) \\ A_3 &= A_2 && (8) \end{aligned}$$

The effective MG dielectric constant ϵ_M is:

$$\epsilon_M = \epsilon_e + \epsilon_e \frac{\frac{v}{3}\sum_{k=1}^{3} f(\epsilon_i, \epsilon_e, A_k)}{1 - \frac{v}{3}\sum_{k=1}^{3} A_k f(\epsilon_i, \epsilon_e, A_k)} \tag{9}$$

where:

$$f(\epsilon_i, \epsilon_e, A_k) = \frac{\epsilon_i - \epsilon_e}{\epsilon_e + A_k(\epsilon_i - \epsilon_e)} \tag{10}$$

By exchanging the role of inclusion and host, two non−intersecting curves are obtained as function of the air volume fraction v. With reference to figure 4, the dashed line is the dielectric constant of an ice host with air inclusions, while the dotted curve is the dielectric constant of an air host with ice inclusions, both as a function of the air volume fraction. The curves do not assume the same value in $v = 0.5$, because of the formula asymmetry and, furthermore, they have slightly different maximum and minimum values for pure ice (clearly they coincide for $v = 1$, i.e. in pure air). But, if it is reasonable that quasi−pure ice (e.g. at firn/ice transition where density is about 830 kg m^{-3}) is “solid ice with air bubbles”, and it is equally meaningful to consider snow as “ice crystals suspended in air”, a transition between the upper and the lower model of Figure 4 must be defined.

The simplest transition is a linear transformation from the former (a/i: air in ice) to the latter (i/a: ice in air), or in other words to compute the mixture dielectric constant ϵ_m as follows, where the inclusion volume fraction has been substituted by the material density ρ which is the parameter of interest:

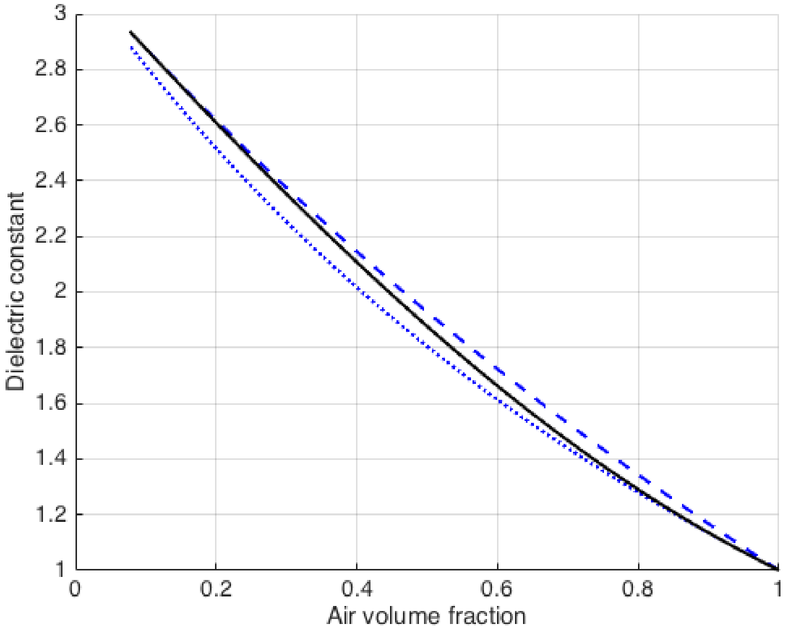

Figure 4: Dielectric constant of an ice/air mixture computed by the MG formula, as a function of the volume fraction (see text)

$$\epsilon_m(\rho) = [1 - \eta(\rho)]\, \epsilon_{i/a}(\rho) + \eta(\rho)\epsilon_{a/i}(\rho) \tag{11}$$

with:

$$\eta(\rho) = \frac{\rho - 1}{\rho_I - 1} \tag{12}$$

Such a linear relation is such that the dielectric constant for $v = 0.5$ is exactly the mean value between those of the upper and lower curves at the same volume fraction. The solid line in figure 4, representing the linear transformation from the a/i to the i/a model, almost perfectly corresponds with the dielectric constant computed by the Bruggeman formula (4), confirming the validity of the linear transformation. Figure 5 shows such a correspondence: the maximum percentage deviation from the Bruggeman formula is less than 0.7 %.

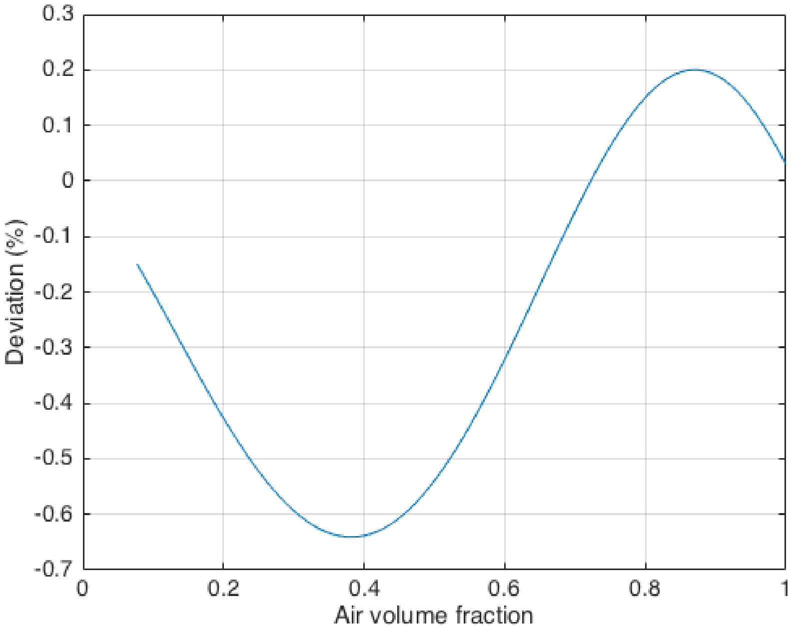

Figure 5: Relative percentage deviation of the linear formula (11) from the Bruggeman effective dielectric constant

5 Results

5.1 Experimental Results

The measurement procedure and, in particular, the electromagnetic model of the open−resonator probe, is described elsewhere (Olmi et al., 2019). Two cavity resonators are used, operating in first and second harmonics.

Briefly summarizing, for each cavity two calibration measurements are conducted − one in air, one with the probe placed on a reference dielectric − at the beginning and at the end of a session (usually half a day), after a full calibration of the vector network analyzer used to measure the transmission through the microwave cavity.

Figure 6 depicts the dielectric constant as function of depth at four frequencies (first and second resonant mode of the two cavity resonators employed), while figure 7 shows the measured loss tangent at the same frequency values. The smooth lines of both dielectric constant and loss tangent are a result of a "smoothed" calibration procedure, not of a direct smoothing or interpolation of the measured data. The transmission coefficient in every session is inverted to give the complex permittivity using the "local" calibration, i.e. that relative to the session (red dots). As an alternative, the calibration parameters at each frequency can be used to build a smoothed calibration curve, which brings to the solid−line values in figures 6 and 7.

It clearly appears that the real part of permittivity weakly depends on frequency and exhibit the same dependence with depth. The same is not true

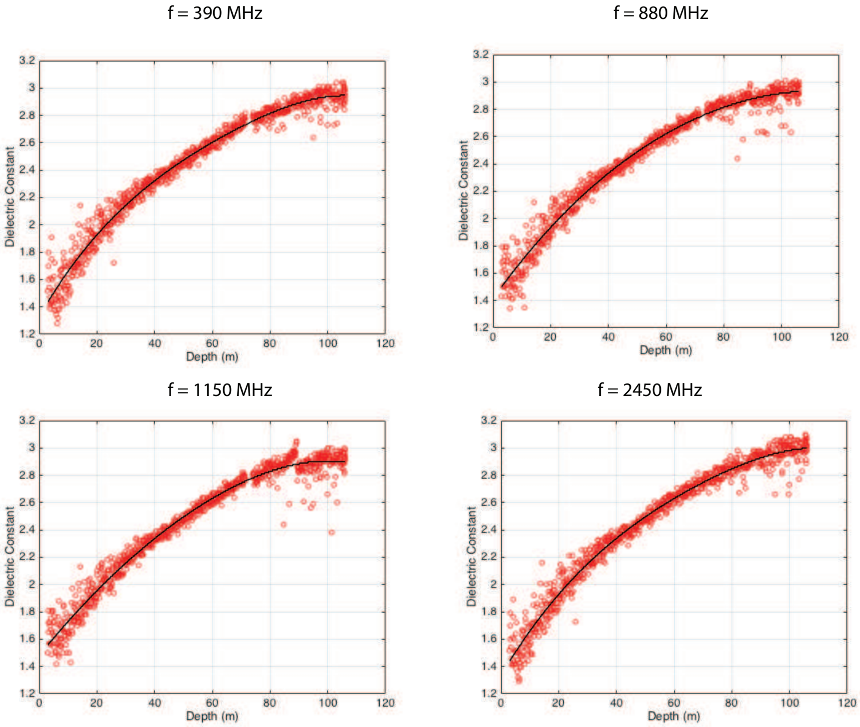

Figure 6: Real part of complex permittivity versus depth

for the imaginary part, whose dependence on frequency appears rather complex, probably due to the presence of salts or impurities, although generally increasing with depth. This could hopefully be confirmed by a cross−check with the findings of physical−chemical analyses currently in progress.

Figure 8 shows the measured density of the core slices as a function of the slice depth. The dependence of density ρ on depth z appears to be described by a power−law relation:

$$\rho(z) = az^b + c \tag{13}$$

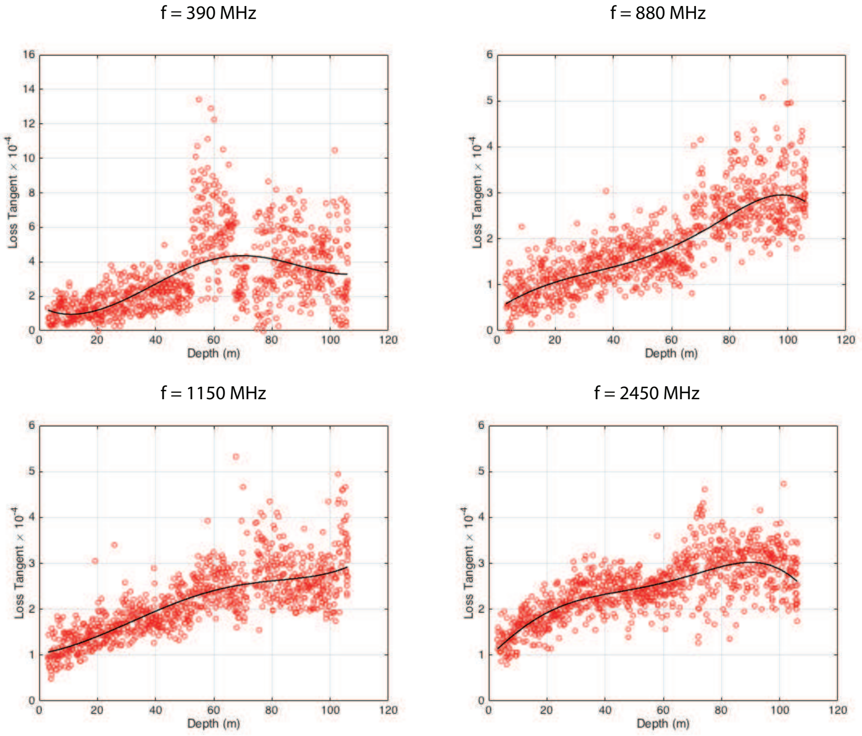

Figure 7: Loss tangent versus depth

which corresponds to the solid line in the figure. The dashed line refers to the bi−exponential fitting model introduced by Arthern et al. (2013), whose rationale is based on the existence of a critical density where a discontinuity appears in the derivative of $\rho(z)$. That kind of relationship does not appear to describe well our experimental data.

5.2 Numerical Results

Two sets of simulations are conducted, to follow the procedure summarized by equation (11). The first set allows to compute $\epsilon_{i/a}(\rho, z)$, the second $\epsilon_{a/i}(\rho, z)$,

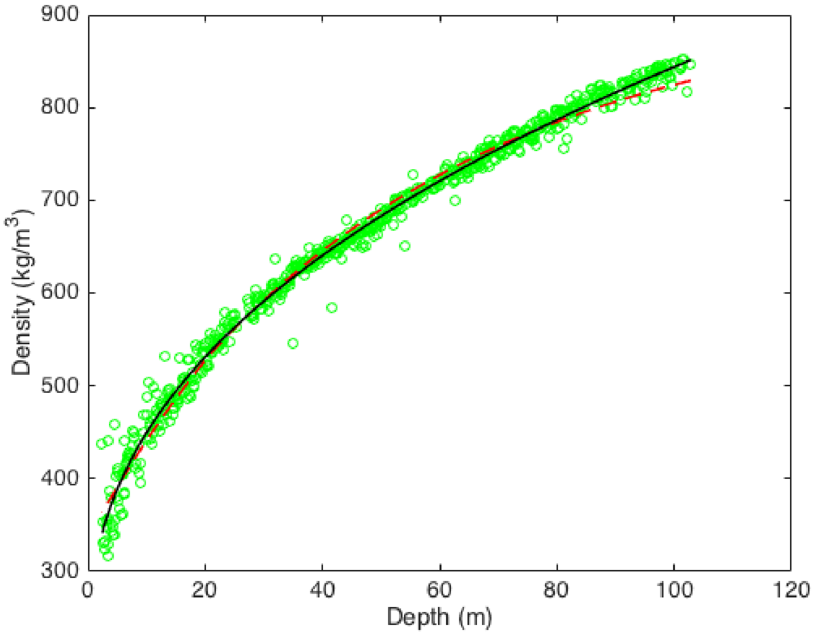

Figure 8: Density $\rho(z)$ versus depth: comparison between the power-law fitting (solid black line) and the bi-exponential fitting (dashed red line)

where "i/a" and "a/i" mean 'ice in air" and "air in ice" respectively, as in Section 4.2.

5.2.1 Statistical Analysis

For each density value (macro−state) we obtain a set of micro−states by the procedure outlined in the previous section. As an example, figure 9 (left) shows a configuration of firn inclusions (black) in air (white) corresponding to a density of 400 kg m^{-3}, and (right) a configuration of air inclusions (white) in a ice host material (black). It is clear from figure 9 how the depth, hence the density, plays a role in the variation of shape and size of the inclusions.

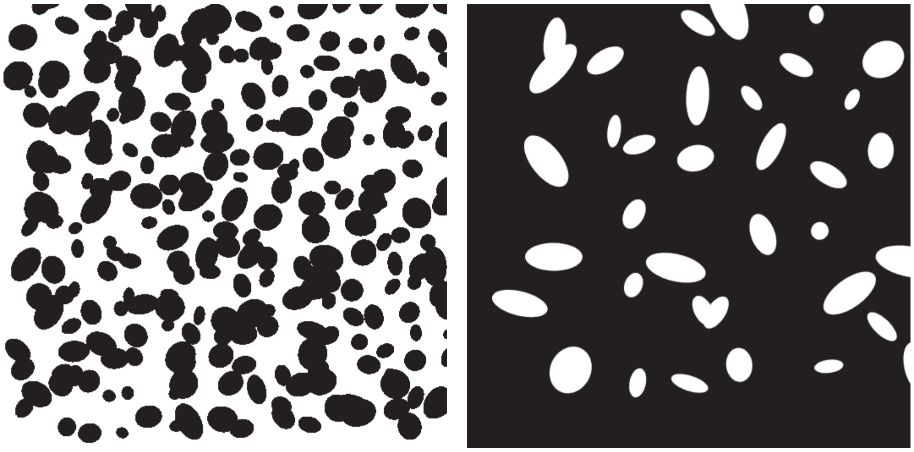

Figure 9: Micro-states. $\rho = 400\,\mathrm{kg\,m^{-3}}$ (left) and $\rho = 800\,\mathrm{kg\,m^{-3}}$ (right)

The density corresponding to a macro−state in a simulation is allowed to have a small interval of variation around the set value, to be able to apply a sort of de−trending to the computed complex permittivity values. In fact, although several formulas exist, see for example Kovacs et al. (1995), relating the real part of permittivity to density and, of course, a fitting of ϵ versus ρ can be performed over the entire density range, we found that greater accuracy in de−trending is achieved by “zooming” into a small region of densities.

Denoting by $\Delta\epsilon'$ and $\Delta\epsilon$” the de−trended values of ϵ' and ϵ”, we obtain from simulations the results presented in Figure 10 for a density of 400 kg m^{-3}.

Very similar results are obtained for a density of 840 kg m^{-3}, as depicted in Figure 11. To summarize, we observe that the dielectric constant (real part) has a 3σ variation of 0.08 for each value in the whole density range. The 3σ

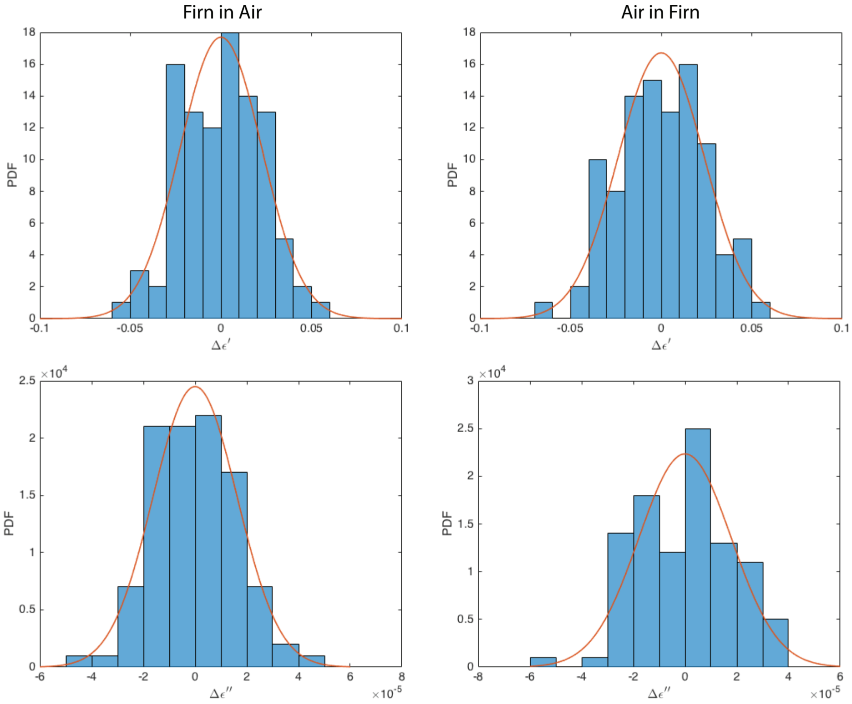

Figure 10: $\Delta\epsilon'$ (top plates) and $\Delta\epsilon$”(bottom plates) for $\rho = 400$ kg m^{-3}

variation is 6×10^{-5} and 9×10^{-5} for dielectric losses at 400 kg m^{-3} and 840 kg m^{-3} respectively. The micro−state variability is entirely responsible of such a variation, as the change with density has been dropped out by the de−trending procedure.

5.2.2 Discussion

Figure 12 compares the experimental results of ϵ as a function of depth with the results of the numerical model. The dashed lines are the $\pm 3\sigma$ values around the mean, i.e. the values between the dashed curves include about 99% of the possible dielectric constants computed by the models as a function of the

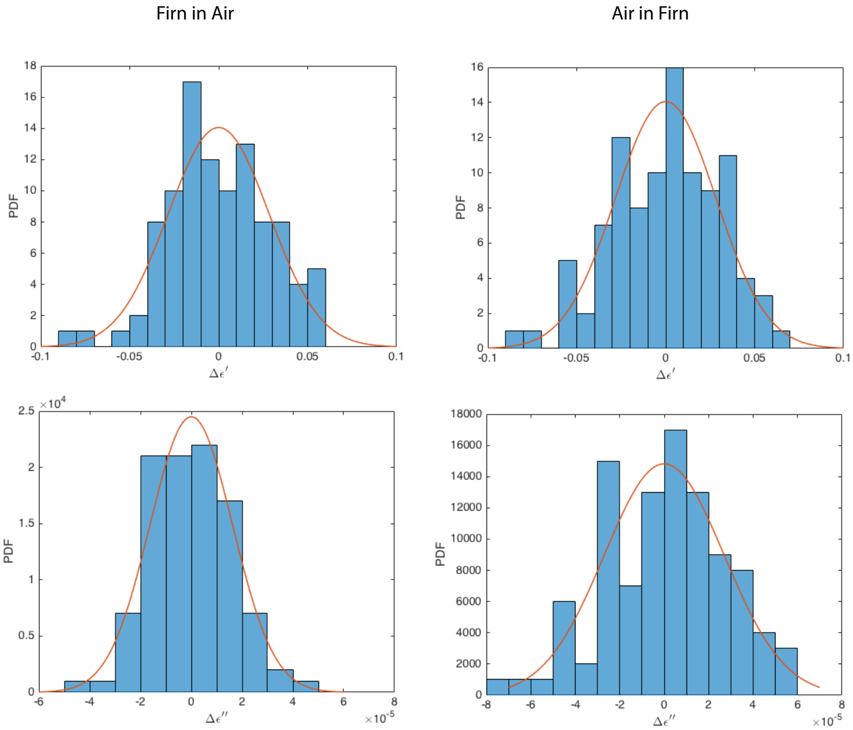

Firn in Air

Air in Firn

Figure 11: $\Delta\epsilon'$ (top plates) and $\Delta\epsilon$"(bottom plates) for $\rho = 840$ kg m^{-3}

micro−state configurations. The solid line is computed applying the linear relation (11), while the dash−dot line is computed by the Bruggeman formula.

The results on the statistical variation of the imaginary part, and hence of the loss tangent, are similar. Of course, the computation of the imaginary part of the ice/air mixture depends on the true value of the imaginary part of pure ice at the frequency of interest, which is not so well defined as the real part (Figure 13). As for the real part, the dashed lines correspond to 3σ variation around the mean value.

The average dielectric constant computed by (11), with the variance based

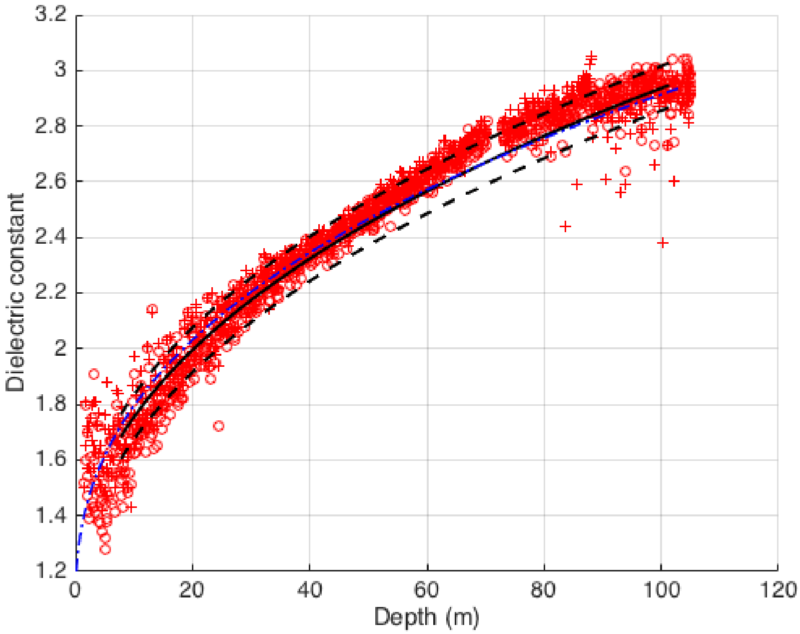

Figure 12: Dielectric constant versus depth: comparison between the experimental data at 880 MHz (red circles) and at 1.15GHz (red crosses) and the results of the full-wave numerical model at 1 GHz

on the statistical analysis, represents quite well the experimental behaviour, like the Bruggeman formula does, only slightly over−estimating the dielectric constant at low depth (lower than 20 meters), i.e. in the lower range of densities. The statistical analysis allows to visualize the expected variability of the average dielectric constant due to the micro−state variability. The variance of the experimental data at a given depth is very similar, although some outliers appear as a consequence of the local variation of density at the close−off depths.

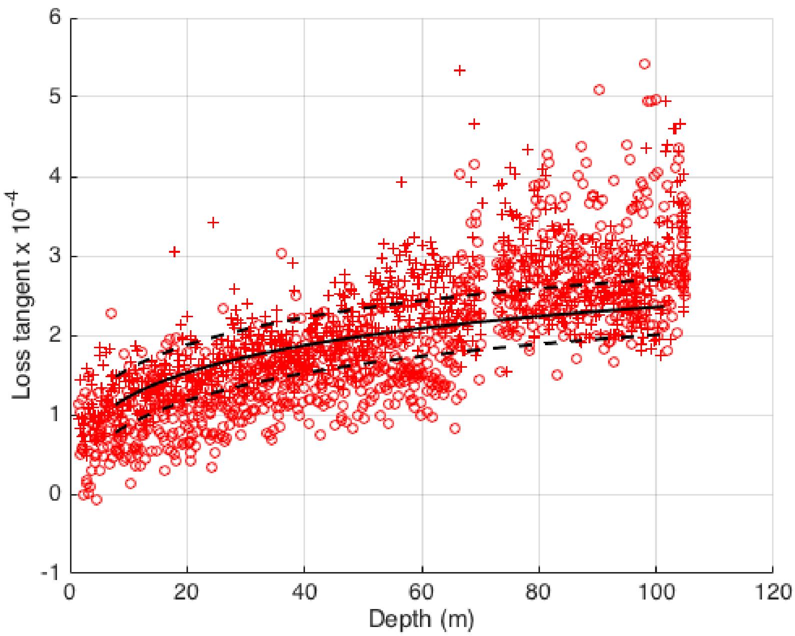

Figure 13: Loss tangent versus depth: comparison between the experimental data at 880 MHz (red circles) and at 1.15GHz (red crosses) and the results of the full-wave numerical model at 1 GHz

6 Conclusions

In this study detailed measurements of firn dielectric properties were performed through the collection of firn cores down to 106 meters, by using a resonator. Detailed measurements of the real and imaginary dielectric permittivity were performed on the ice cores providing an extended dataset of dielectric properties with depth. Density was also measured for the same samples. The experimental results confirmed the dependence of the real part with depth and density. Increasing depth and density corresponds to an increase in the real permittivity.

A power−law equation was derived to fit the data. The imaginary part also increases with depth but it does not follow the same clear trend, its dependence on frequency appears rather complex, probably due to the presence of salts or impurities.

The analysis of the experimental data was performed by first implementing 3D and 2D full wave numerical models, by generating random ensembles of inclusions , to simulate a mixture of firn crystals at prescribed densities, corresponding to the measured densities on the ice cores. The numerical analysis of the ensemble of inclusions showed that the common symmetric functions used for ice dielectric properties do not agree with the results of the simulation and with the measured data. These results show that a host of ice crystals into air significantly differs from a host of air bubbles into ice, and therefore non−symmetric formulations should be used. A single non−symmetric formulation is not sufficient to continuously represent the whole density range. Moreover, analytical formulae are unable to account for the effect of randomness, size/shape heterogeneity, particle packing on the average firn permittivity.

To solve this problems a dielectric model was developed, allowing for quantification of the dependence of the dielectric properties on density. The model was developed by combining two models: one of firn crystals into an air host, and air inclusions into an ice host. The weighted equation is based on the volume fraction (density). The result is a mixture smoothly changing from firn particles in air (low density) to air bubbles in an ice matrix (high density). The implementation of such a mixture model by means of a numerical model allowed to investigate the dependence of complex permittivity at all densities in the range 350−840 kg m^{-3}, on the average firn characteristics, e.g. crystal area, shape and orientation, and on the average crystal arrangement. For this purpose, a statistical analysis has been conducted showing how the variability of the micro−states affects the average permittivity. The permittivity change due to micro−state variability appears to be at least two−three times that due to the measured variability of density at a given depth, therefore concluding that firn structure has a significant effect on the dielectric properties.

7 Acknowledgement

This study was funded by PNRA (Progetti Nazionali di Ricerca in Antartide, Ministry of Education and Research, Rome, Italy) Research Project: Dielectric Characterization of the Polar Cap by perforations at Dome−C (PNRA16-00212), and by the Institut Paul Emile Victor (France). The ice core was obtained from the Centre de Carottage et de Forage National (France).

References

Arnaud, L., Barnola, J., Duval, P., 2000. Physical modelling of the densification of snow/firn and ice in the upper part of polar ice sheets, In: Physics of Ice Core Records, Hokkaido Univ. Press, Sapporo, Japan., pp. 285–305.

Arnaud, L., Lipenkov, V., Barnola, M., Gay, M., Duval, P., 1998. Modelling of the densification of polar firn: characterization of the snow-firn transition. Annals of Glaciology 26, 39–44.

Arthern, R.J., Corr, H.F.J., Gillet-Chaulet, F., Hawley, R.L., Morris, E.M., 2013. Inversion for the density-depth profile of polar firn using a stepped-frequency radar. Journal of Geophysical Research: Earth Surface 118, 1257–1263.

Azuma, N., Wang, Y., Mori, K., Narita, H., Hondoh, T., Shoji, H., Watanabe, O., 1999. Texture and fabrics in the dome f (antarctica) ice core. Annals of Glaciology 29, 163–168.

Cuffey, K., Paterson, W., 2010. The physics of glaciers. volume ISBN 978-0-12-369461-4. fourth ed., Elsevier, Amsterdam.

Grimm, E., D.E.Stillman, MacGregor, J., 2015. Dielectricsignaturesand evolutio nof glacier ice. J. Glaciol. 61, 1159–1170.

Jun, L., Jacka, T.H., 1999. Crystal-growth rates in firn and shallow ice at high-accumulation sites. Annals of Glaciology 29, 169–175.

Karkkainen, K.K., Sihvola, A.H., Nikoskinen, K.I., 2000. Effective permittivity of mixtures: Numerical validation by the fdtd method. IEEE Trans. on Geosci. and Remote Sens. 38, 1303–1308.

Koledintseva, M.Y., Chandra, S.K.R., DuBroff, R.E., Schwartz, R.W., 2006. Modeling of dielectric mixtures containing conducting inclusions with statistically distributed aspect ratio. Progress In Electromagnetics Research 66, 213–228.

Kovacs, A., Gow, A.J., Morey, R.M., 1995. The in-situ dielectric constant of polar firn revisited. Cold Regione Science and Technology 23, 245–256.

Lipenkov, V.Y., Barkov, N.I., Duval, P., Pimienta, P., 1989. Crystalline texture of the 2083 m ice core at vostok station, antarctica. Journal of Glaciology 35, 392–398.

Matzer, C., 1996. Microwave permittivity of dry snow. IEEE Trans. Geo. Remote Sens. 34, 573–581.

Moore, J., 1988. Dielectric variability of a 130 m antarctice ice core: Implications for radar sounding. Annals of Glaciology 11, 95–99.

Olmi, R., Toccafondi, A., Priori, S., Puggelli, F., 2019. An open-resonator sensor for measuring the dielectric properties of antarctic ice. Sensors 19, 2099.

Polder, D., van Santen, J.H., 1946. The effective permeability of mixtures of solids. Physica 12, 257–271.

Sihvola, A., 1999. Electromagnetic Mixing Formulas and Applications. Electromagn. waves ser. 47, ed., Inst. Electr. Eng., London.

Sihvola, A.H., 2000. Mixing rules with complex dielectric coefficients. Subsurface Sensing Technologies and Applications 1, 393–415.

Suguyama, S., Enomoto, H., Fujita, S., Fukui, K., Nakazawa, F., Holmlund, P., 2010. Dielectric permittivity of snow measured along the route traversed in the japanese-swedish antarctic expedition 2007/08. Annals of Glaciology 51, 9–15.

Tiuri, M., Sihvola, A., Nyfors, E., Hallikaiken, M., 1984. The complex dielectric constant of snow at microwave frequencies. IEEE Journal of Oceanic Engineering OE-9.

Tuncer, E., Gubanski, S.M., Nettelblad, B., 2001. Dielectric relaxation in dielectric mixtures: Application of the finite element method and its comparison with dielectric mixture formulas. Journal of Applied Physics 89, 8092–8100.

Wolff, E., 2000. Electrical stratigraphy of polar ice cores: Principles, methods, and findings, in: Hondoh, T. (Ed.), Physics of Ice Core Records. Hokkaido Univ. Press, Sapporo, Japan, p. 155–171.

Wolff, E., Miners, W., Moore, J.C., Paren, J.G., 1997. Factors controlling the electrical conductivity of ice from polar regions—a summary,. J. Phys. Chem. B 101, 6090– 6094.

Zhao, X., Wu, Y., Fan, Z., Li, F., 2004. Three-dimensional simulations of the complex dielectric properties of random composites by finite element method. Journal of Applied Physics 95, 8110–8117.

Declaration of interests

☒ The authors declare that they have no known competing financial interests or personal relationships that could have appeared to influence the work reported in this paper.

☐The authors declare the following financial interests/personal relationships which may be considered as potential competing interests: